

Supporting Information

Two Exceptional Homoleptic Iron(IV) Tetraalkyl Complexes

*Alicia Casitas, Julian A. Rees, Richard Goddard, Eckhard Bill, Serena DeBeer, and
Alois Fürstner**

anie_201612299_sm_miscellaneous_information.pdf

Single-Crystal X-ray Structure Analysis of [Fe(cyclohexyl)₄] (**4**)

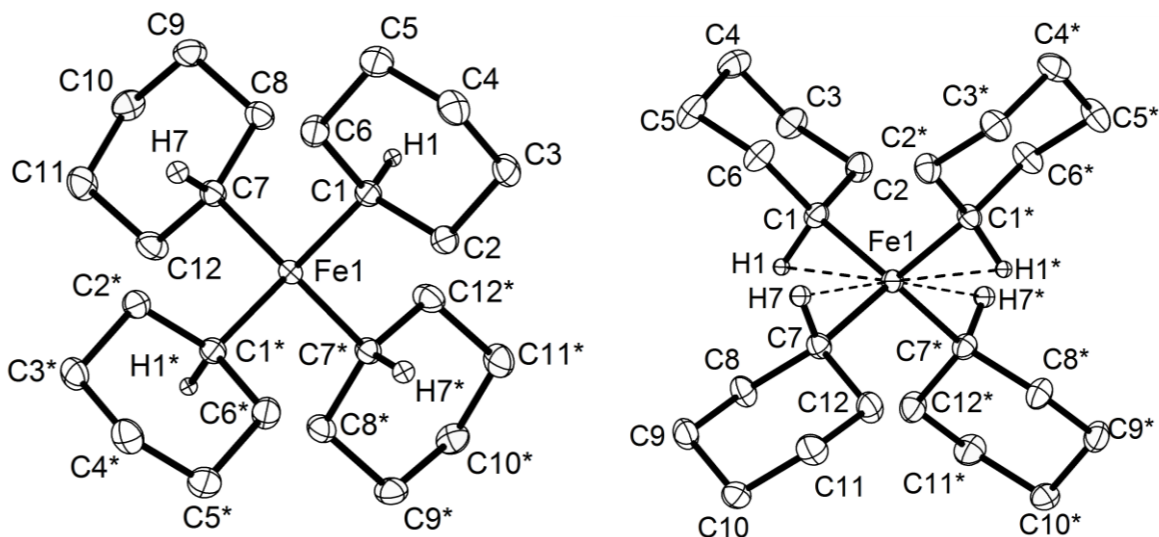


Figure S1. Two views of the molecular structure of [Fe(cyclohexyl)₄] (**4**). Methylene H atoms are removed for clarity.

X-ray Crystal Structure Analysis of [Fe(cyclohexyl)₄] (4**):** C₂₄H₄₄Fe, $M_r = 388.44 \text{ g} \cdot \text{mol}^{-1}$, purple prism, crystal size 0.05 x 0.07 x 0.08 mm³, monoclinic, space group *C2/c*, $a = 17.3581(4) \text{ \AA}$, $b = 8.3613(3) \text{ \AA}$, $c = 17.2442(5) \text{ \AA}$, $\beta = 118.873(4)^\circ$, $V = 2191.65(13) \text{ \AA}^3$, $T = 100(2) \text{ K}$, $Z = 4$, $D_{calc} = 1.177 \text{ g} \cdot \text{cm}^{-3}$, $\lambda = 0.71073 \text{ \AA}$, $\mu(\text{Mo-K}\alpha) = 0.692 \text{ mm}^{-1}$, Gaussian absorption correction ($T_{min} = 0.92459$, $T_{max} = 0.97077$), Bruker AXS Enraf-Nonius KappaCCD diffractometer, $2.780 < \theta < 33.116^\circ$, 26415 measured reflections, 4163 independent reflections, 3746 reflections with $I > 2\sigma(I)$, $R_{int} = 0.037$.

INTENSITY STATISTICS FOR DATASET

Resolution	#Data	#Theory	%Complete	Redundancy	Mean I	Mean I/s	Rmerge	Rsigma
Inf - 2.72	66	73	90.4	10.19	105.4	72.41	0.0362	0.0143
2.72 - 1.82	154	154	100.0	9.40	80.3	65.67	0.0304	0.0130
1.82 - 1.42	224	224	100.0	8.63	52.3	58.56	0.0280	0.0134
1.42 - 1.24	223	223	100.0	8.38	43.3	57.85	0.0280	0.0137
1.24 - 1.12	234	234	100.0	7.83	27.1	45.33	0.0276	0.0161
1.12 - 1.04	208	208	100.0	7.46	22.3	38.71	0.0326	0.0183
1.04 - 0.98	212	212	100.0	7.33	16.3	34.95	0.0341	0.0205
0.98 - 0.93	219	219	100.0	6.83	16.7	34.46	0.0347	0.0220
0.93 - 0.88	267	267	100.0	6.55	14.6	30.46	0.0387	0.0243
0.88 - 0.85	203	203	100.0	6.14	12.9	26.60	0.0424	0.0270
0.85 - 0.82	226	226	100.0	5.99	12.2	26.06	0.0471	0.0299
0.82 - 0.79	255	255	100.0	5.73	9.6	21.44	0.0533	0.0345
0.79 - 0.77	195	195	100.0	5.41	8.6	20.04	0.0582	0.0382
0.77 - 0.75	214	214	100.0	5.28	7.5	17.58	0.0685	0.0430
0.75 - 0.73	238	238	100.0	5.11	6.5	15.08	0.0728	0.0479
0.73 - 0.71	271	271	100.0	4.83	6.4	14.70	0.0786	0.0518
0.71 - 0.70	139	139	100.0	4.63	7.0	15.30	0.0788	0.0515
0.70 - 0.68	315	316	99.7	4.52	5.6	12.70	0.0910	0.0606
0.68 - 0.67	184	184	100.0	4.42	5.2	11.70	0.0943	0.0647
0.67 - 0.66	176	176	100.0	4.14	5.0	11.50	0.0971	0.0720
0.66 - 0.65	179	181	98.9	4.10	4.9	11.21	0.1018	0.0743

0.75 - 0.65	1502	1505	99.8	4.57	5.8	13.24	0.0855	0.0586
Inf - 0.65	4402	4412	99.8	6.19	18.7	28.84	0.0368	0.0226

The structure was solved by direct methods and refined by full-matrix least-squares against F^2 to $R_1 = 0.031$ [$I > 2\sigma(I)$], $wR_2 = 0.090$, 122 parameters. The α -carbon H atoms were refined with isotropic atomic displacement parameters, otherwise H atoms were refined using a riding model with a C-H distance of 0.99 Å and $U_H = 1.2 \times U_C$, $S = 1.136$, residual electron density 0.44 (0.70 Å from C9)/ -0.48 (0.58 Å from Fe1) $e \text{ \AA}^{-3}$. **CCDC-1519438**.

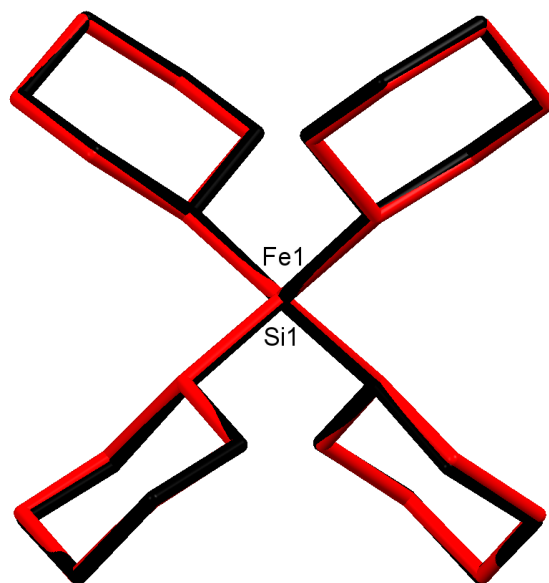


Figure S2. Superposition of $[\text{Fe}(\text{cyclohexyl})_4]$ and $[\text{Si}(\text{cyclohexyl})_4]$ (CSD refcode: TCYHSI). The rms deviation for non-H atoms is 0.0616 Å.

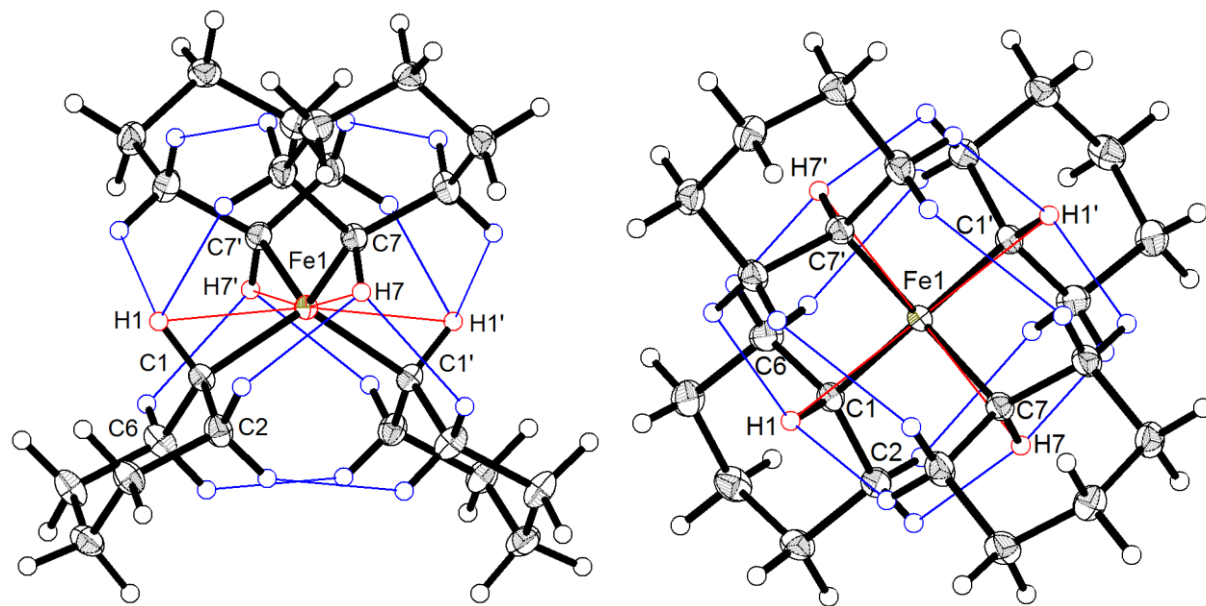


Figure S3. Steric interactions in $[\text{Fe}(\text{cyclohexyl})_4]$ (blue: $\text{H}\cdots\text{H}$ distances < 2.4 Å; red: $\text{Fe}\cdots\text{H}$ distances < 2.3 Å).

Preparative Data

[Fe(cyclohexyl)₄]. A flame-dried Schlenk flask equipped with a magnetic stirring bar was charged under Ar with Fe(acac)₂ (370 mg, 1.456 mmol) and THF (20 mL). The resulting solution was cooled to –35°C before cyclohexylmagnesium chloride (2 M in Et₂O, 1.45 mL, 2.90 mmol)¹ was added dropwise. The resulting dark mixture was stirred at this temperature for 3 h before all volatile components were removed in high vacuum. The black residue was triturated with pentane (ca. 250 mL) and the resulting suspension filtered at –35°C to afford a clear magenta-colored solution. Evaporation of the solvent at –35°C in high vacuum afforded the title complex as a dark red solid material (131 mg, 23%). Single crystals suitable for X-ray diffraction were grown by slowly cooling a solution of the complex in the minimum amount of pentane to –78°C. ¹H NMR (400 MHz, [D₈]-toluene, –30°C): δ = 2.54 (m, 4H), 1.84-1.56 (m, 20H), 1.52-1.38 (m, 8H), 1.38-1.19 (m, 6H), 0.93-0.72 ppm (m, 6H); ¹³C NMR (101 MHz, [D₈]-toluene, –50°C): δ = 52.8, 35.07, 28.0, 27.9 ppm; Analysis calcd. for C₂₄H₄₄Fe: C 74.21, H 11.42; found: C 74.50, H 11.32.

[Fe(2-adamantyl)₄]. A flame-dried Schlenk flask equipped with a magnetic stirring bar was charged under Ar with FeCl₂·(thf)_{1.5} (106 mg, 0.45 mmol) and THF (5 mL). The resulting solution was cooled to –50°C before a solution of 2-adamantyllithium (0.1 M in Et₂O, 13 mL, 1.30 mmol) was slowly added via canula. Once the addition was complete, the mixture was stirred overnight at –70°C before the solution was concentrated to ca. 1/3 of the original volume. The solid material was allowed to settle. The supernatant was carefully decanted and the remaining material successively washed with cold THF and cold pentane (–70°C each) to leave the title complex behind as a magenta-colored solid material (70 mg, 26%). Anal. calcd. for C₄₀H₆₀Fe: C 80.51, H 10.13; found: C 80.23, H 10.33.

Mössbauer Spectroscopy

Mössbauer spectra were recorded on a conventional spectrometer with alternating constant acceleration of the γ -source. The minimum experimental line width was 0.24 mm/s (full width at half-height). The sample temperature was maintained constant in an Oxford Instruments Variox or in an Oxford Instruments Mössbauer-Spectromag cryostat. The latter is a split-pair super-conducting magnet system for applied fields up to 8 T where the temperature of the sample can be varied in the range 1.5 K to 250 K. The field at the sample is perpendicular to the γ -beam. The ⁵⁷Co/Rh source (1.8 GBq) was positioned at room temperature inside the gap of the magnet system at a zero-field position, by using a re-entrant bore. Isomer shifts are quoted relative to iron metal at 300 K. Magnetic Mössbauer spectra were simulated with the program MX (by E.B.) with electronic spin $S = 0$ and the usual nuclear Hamiltonian^[1] for the calculation of the hyperfine interaction for ⁵⁷Fe.

¹ The use of 4 equivalents of cyclohexylmagnesium chloride led to almost the exact same yield (24%).

X-ray Emission Spectroscopy

Fe K β X-ray emission spectra were collected at beamline C-1 at the Cornell High Energy Synchrotron Source (CHESS). A solid sample of **4** was placed in a mortar cooled by liquid N₂, and a pre-cooled pestle was used to grind the solid into a fine powder. The powder was transferred to a 1 mm thick Al spacer taped to an LN₂-cooled Al block, and sealed in place using 38 μ m Kapton tape. The sample was then placed in a shipping dewar and transported and handled at cryogenic temperatures. During measurements, the sample was placed in the slotted Cu cold head of a closed-cycle He cryostat and maintained at 40 K in a reduced pressure atmosphere. Data were collected with a ring current of 110 mA and a ring energy of 5.3 GeV, operating in 90 minute decay mode. Using a pair of W/B₄C multilayers, the incident energy was set to approximately 9 keV with a \sim 1% bandwidth. The beam spot size on the sample was 2.0 x 1.0 mm², and the photon flux on the sample was roughly 2.6 x 10¹² photons / sec. The Fe K β X-ray fluorescence was analyzed using an array of 5 spherically-bent Ge(620) crystals and detected using a Dectris 100K, arranged in a Rowland geometry as previously described.^[2] A digital region of interest (ROI) was selected to tightly enclose the reflections of all 5 crystals throughout the scan range, and a concentric ROI of 4 times the size was also specified for background subtraction. Data analysis was performed using MATLAB. The energy axis was calibrated using the K β emission features of Fe₂O₃ (K β ' = 7045.2 eV, K β _{1,3} = 7060.6 eV, K β '' = 7092.0 eV, K β _{2,5} = 7107.2 eV), and the background-corrected spectrum of **4** was obtained by subtracting the difference between smaller and larger ROI intensities from the smaller ROI intensity. The total integrated spectral area was normalized to 1000. The experimental data were fit using a sum of pseudo-Voigt profiles, and the parameters of the profiles (peak position, integrated area, full width at half max, and the fraction of Gaussian and Lorentzian lineshapes) were optimized to fit the experimental data using the trust-region algorithm. The profiles underlying the mainline region (7030 – 7080 eV) were summed to obtain the mainline background, which is shown as the red dashed trace in the VtC region in Figure 3.

Electronic Absorption

Electronic absorption measurements have been performed with a Cary 8454 UV-vis diode-array spectrometer from Agilent Technologies. The sample was dissolved in THF (7.39 mM), and the sample temperature was maintained constant at -30°C in a home-built quartz cuvette (1 cm path length) with vacuum jacket. The cuvette was cooled with a flow of ethanol stabilized by a Lambda Master Pro Line RP 1290 cryo-cooler.

Compound **4** dissolved in THF is of pale 'reddish' color and shows a UV-vis absorption spectrum with a dominant band at \sim 36150 cm⁻¹ (Figure S4), which we assigned to LMCT transitions. In addition, two weak ligand-field transitions could be detected at 18052 and 20210 cm⁻¹. According to the Tanabe-Sugano diagrams for 3d⁴ low-spin configuration in tetrahedral symmetry these can be nicely assigned to the two spin-allowed ¹A₁ \rightarrow ¹T₁ and ¹A₁ \rightarrow ¹T₂ transitions from the ¹A₁ orbital singlet ground state of the Fe(IV) compound (equivalent to the situation for the 3d⁶ low-spin configuration in octahedral symmetry, as often encountered e.g. for Co(III)).² The relatively high values of these *d-d* transitions is in accord with the unusual low-spin state of the compound, which otherwise is rarely seen in four coordinate

² Compare: J. S. Griffith, *The Theory of Transition-Metal Ions*; Cambridge University Press: Cambridge, 1961.

tetrahedral complexes. Time-dependent-DFT calculations corroborate the band assignment, showing a set of weak transitions at $\approx 17,100\text{ cm}^{-1}$ and stronger transitions at $\approx 23,000\text{ cm}^{-1}$. These accord with the experimental data well within the acceptable margin of error.

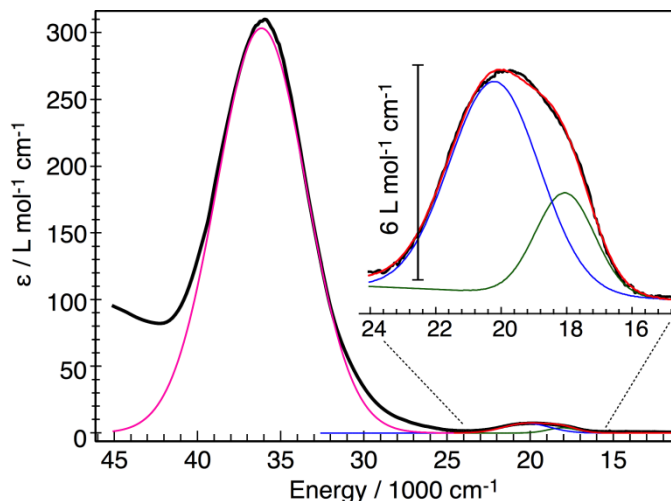


Figure S4. Electronic absorption spectrum of **4** in THF solution (black line); the red line is a simulation with three Gaussian centered at 18052 cm^{-1} (green), 20210 cm^{-1} (blue), and 36147 cm^{-1} (magenta) with line widths of 1800 , 2745 , and 5400 cm^{-1} , respectively.

DFT Calculations. All DFT calculations were performed using the ORCA program package, v. 3.0.3.^[3] Calculations utilized the def2-TZVP and auxiliary def2-TZVP/J basis sets,^[4,5] a dense integration grid (Grid5), an especially dense integration grid on iron (Grid7), and tight SCF convergence criteria were required. Geometry optimizations were performed using the B3PW91^[6,7] hybrid density functional with the RIJCOSX approximation,^[8-10] both with and without the D3BJ dispersion correction.^[11,12] The geometry optimization of **4** was initiated from the crystallographic coordinates, and the starting structure of **5** was generated by replacing the cyclohexyl ligands with adamantyl groups *in silico*. The calculations of X-ray emission spectra (**4**) and Mössbauer parameters (**4** and **5**) were performed using the geometries optimized without D3BJ (where the metrical parameters more closely agreed with experiment in the case of **4**), and used the BP86 density functional^[13,14] and the special CP(PPP) core properties basis set^[15] on iron. Calculated X-ray emission energies were calculated as the difference in Kohn-Sham orbital energies between the donor and acceptor (Fe 1s) orbitals, and intensities were obtained by summing the calculated electric and magnetic dipole and electric quadrupole contributions to oscillator strength.^[16] The molecular orbital fragment analysis was performed using MOAnalyzer,^[17] and molecular orbital isosurfaces were visualized with Chimera (UCSF).^[18] The ^{57}Fe Mössbauer quadrupole splitting is given in the output file of the nuclear properties calculation, however the calculated isomer shift was obtained from the electron density ρ at the nucleus using the calibration parameters reported by Römelt et al.^[19]

TD-DFT calculations were performed using the B3LYP hybrid density functional and the RIJCOSX approximation, with otherwise identical parameters to those detailed previously.

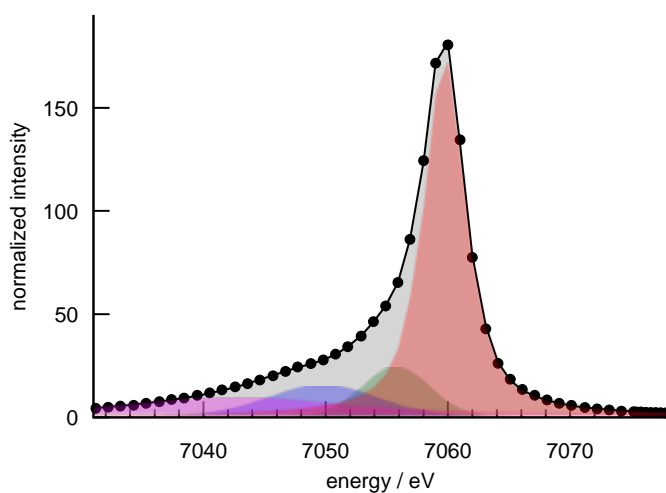


Figure S5. Mainline region of the Fe K β X-ray emission spectrum of **4**. Black dots are experimental data, black line is the total fit to the data, and the colored pseudo-Voigt profiles are the component functions of the fit.

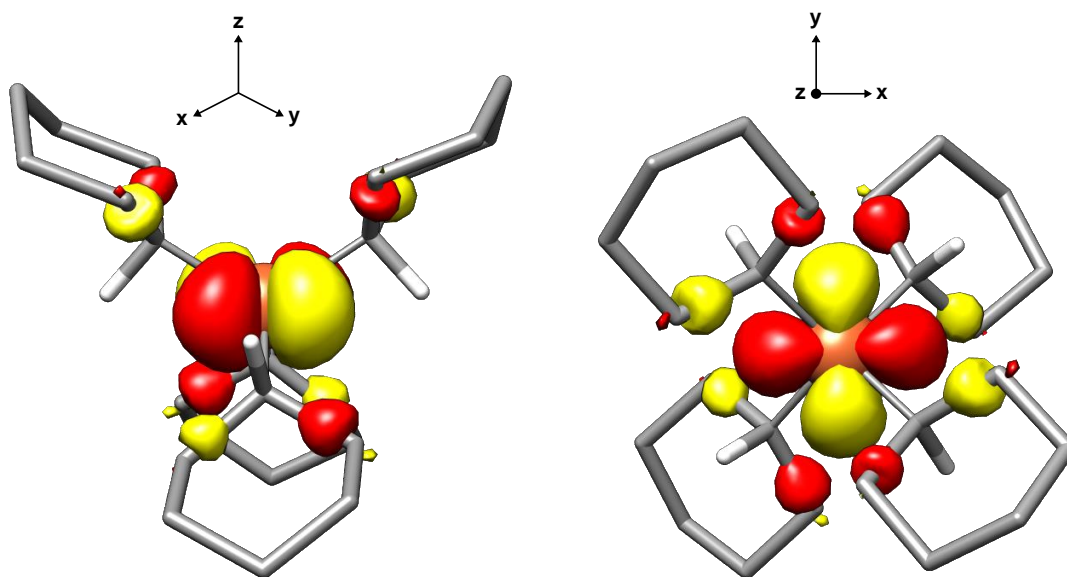


Figure S6. DFT-calculated molecular orbital assigned as $3d_{x^2-y^2}$. Due to the orientation, it is non-bonding with both the lone pair on the α -C and the α -H. It displays antibonding interactions with the α -C – β -C bond. Molecular orbital isosurfaces are shown at an isovalue of $0.035 a_0^{-3/2}$

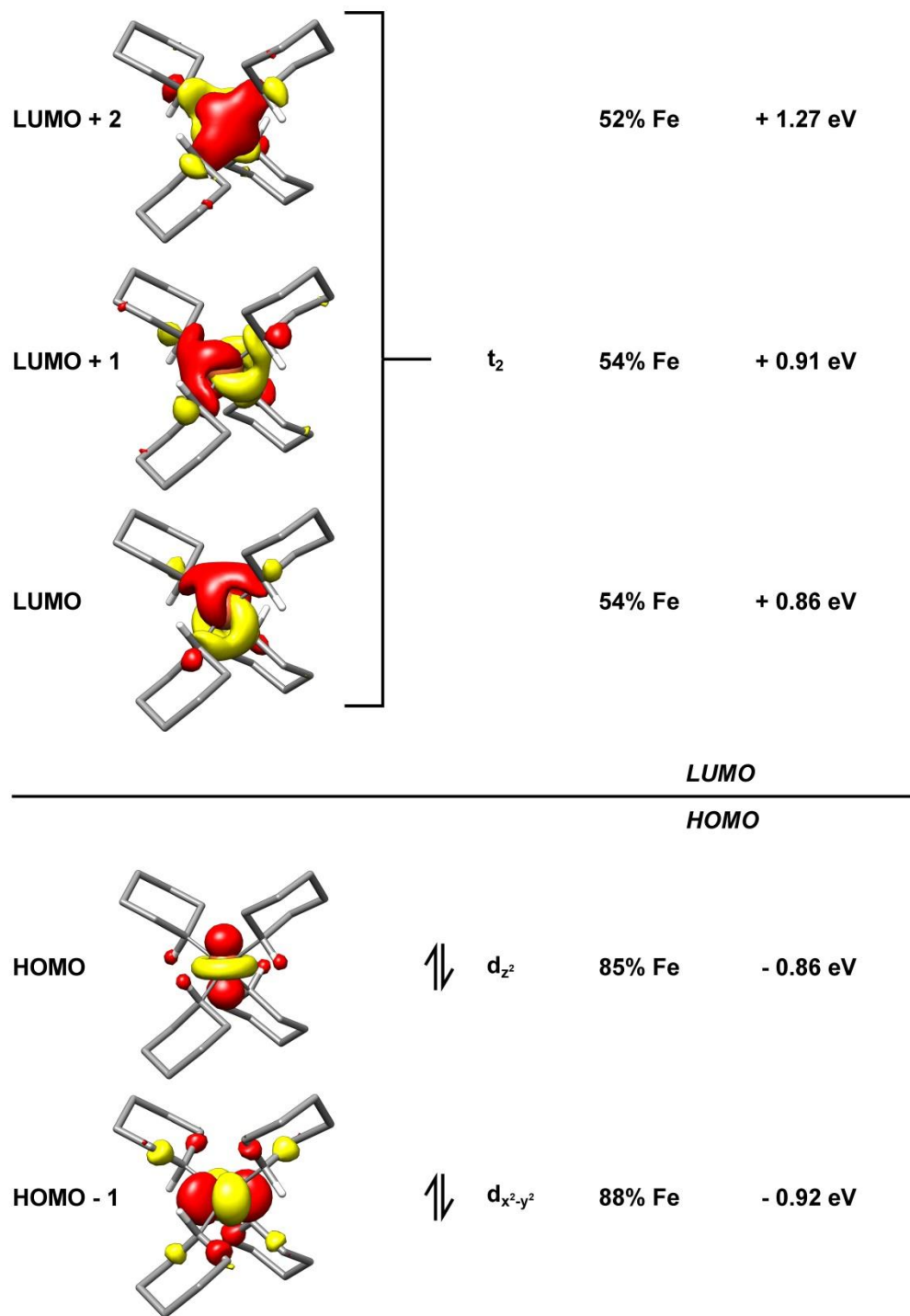


Figure S7. Molecular orbital diagram of complex **4**. The calculated orbital energies and the percent Fe contribution to each Kohn-Sham orbital are given. The midpoint of the HOMO-LUMO gap has been normalized to 0 eV, and the orbitals are shown at an isovalue of $0.05 a_0^{-3/2}$.

- [1] P. Gütllich, E. Bill, A. X. Trautwein, *Mössbauer Spectroscopy and Transition Metal Chemistry*, Springer Berlin Heidelberg, Berlin, Heidelberg, **2011**.
- [2] K. D. Finkelstein, C. J. Pollock, A. Lyndaker, T. Krawczyk, J. Conrad, **2016**, p. 30009, [dx.doi.org/10.1063/1.4952832](https://doi.org/10.1063/1.4952832)
- [3] F. Neese, *Wiley Interdiscip. Rev. Comput. Mol. Sci.* **2012**, *2*, 73–78.
- [4] F. Weigend, R. Ahlrichs, *Phys. Chem. Chem. Phys.* **2005**, *7*, 3297–3305.
- [5] A. Schäfer, H. Horn, R. Ahlrichs, *J. Chem. Phys.* **1992**, *97*, 2571–2578.
- [6] A. D. Becke, *J. Chem. Phys.* **1993**, *98*, 5648.
- [7] J. P. Perdew, *Electronic Structure of Solids '91*, Akademie Verlag, Berlin, **1991**.
- [8] B. I. Dunlap, J. W. D. Connolly, J. R. Sabin, *J. Chem. Phys.* **1979**, *71*, 3396–3402.
- [9] M. Feyereisen, G. Fitzgerald, A. Komornicki, *Chem. Phys. Lett.* **1993**, *208*, 359–363.
- [10] F. Neese, F. Wennmohs, A. Hansen, U. Becker, *Chem. Phys.* **2009**, *356*, 98–109.
- [11] S. Grimme, S. Ehrlich, L. Goerigk, *J. Comput. Chem.* **2011**, *32*, 1456.
- [12] S. Grimme, J. Antony, S. Ehrlich, H. Krieg, *J. Chem. Phys.* **2010**, *132*, 154104.
- [13] A. . Becke, *Phys. Rev. A* **1988**, *38*, 3098–3100.
- [14] J. P. Perdew, *Phys. Rev. B* **1986**, *33*, 8822–8824.
- [15] F. Neese, *Inorg. Chim. Acta* **2002**, *337*, 181–192.
- [16] N. Lee, T. Petrenko, U. Bergmann, F. Neese, S. DeBeer, *J. Am. Chem. Soc.* **2010**, *132*, 9715–9727.
- [17] M. U. Delgado-Jaime, S. DeBeer, *J. Comput. Chem.* **2012**, *33*, 2180–2185.
- [18] E. F. Pettersen, T. D. Goddard, C. C. Huang, G. S. Couch, D. M. Greenblatt, E. C. Meng, T. E. Ferrin, *J. Comput. Chem.* **2004**, *13*, 1605.
- [19] M. Römel, S. Ye, F. Neese, *Inorg. Chem.* **2009**, *48*, 784–785.